Frequency Scaling Millimeter Wave Acoustic Resonators using Ion Beam Trimmed Lithium Niobate

Vakhtang Chulukhadze[†], Kenny Huynh [‡], Jack Kramer[†], Michael Liao[‡], Sinwoo Cho[†], Lezli Matto[‡], Omar A. Barrera[†], Can Cui[†], Mark S. Goorsky[‡], and Ruochen Lu[†]
[†]Department of Electrical and Computer Engineering, The University of Texas at Austin, Austin, TX, USA
[‡]Department of Materials Science & Engineering, University of California, Los Angeles, CA, USA

***Summary*—This paper reports a method of frequency scaling millimeter wave thin-film lithium niobate ($LiNbO_3$) acoustic resonators using ion beam assisted Argon gas cluster trimming whilst maintaining a high figure of merit (FoM) and averting ultra-thin-film fabrication difficulties. A transferred 100 nm thick 128° Y-cut $LiNbO_3$ thin film is trimmed to a thickness of 75 nm. Consequently, a 24.4 GHz first-order antisymmetric mode (A1) resonator with a high k^2 of 34.3%, a Q of 54, and an FoM of 18.5 is presented. The quality of the film was maintained during the trimming process, proven by material-level analysis, and exhibited a similar $f \cdot Q$ product compared with resonators fabricated using the original film. These results show a viable and less complex path toward further frequency scaling acoustic devices.**

Keywords—lithium niobate, thin-film devices, millimeter wave acoustic resonator, ion beam etching

I. Introduction

Radio frequency acoustic resonators are highly sought after due to better energy confinement along with a smaller footprint compared to their electromagnetic (EM) counterparts [1], [2]. Built upon the success of piezoelectric devices operating at sub-6-GHz, researchers are exploring acoustic devices in the millimeter wave (mm-wave) regime for future 5G/6G systems. Examples of material systems from which these devices have been fabricated include lithium niobate ($LiNbO_3$)[3]–[6], aluminum nitride (AlN) [7], [8], and scandium aluminum nitride (ScAlN) [9]. However, scaling acoustics into mm-wave is challenging due to fabrication difficulties and the significant attenuation associated with ultra-thin films (sub-100 nm). Sputtered materials suffer from moderate film orientation near substrate [9]; epitaxially grown materials cannot achieve high quality on silicon and are thus difficult to release [10]; and transferred ultra-thin films suffer from poor uniformity [11]. Furthermore, $LiNbO_3$ is considered a material that is difficult to dry etch, with many attempts leading to increased surface roughness and sub-wavelength scattering [12]. The conventional approach to etching $LiNbO_3$ is by inductively coupled plasma reactive ion etching (ICP-RIE). While ICP-RIE can deliver a high etch rate for the material, it cannot minimize electrostatic damage imparted to the film, leading to moderate surface and sidewall roughness which is detrimental to device performance [13]. An alternative to ICP-RIE is chemical wet etching, increasing the throughput and decreasing the cost of etching $LiNbO_3$. While several formulae have been developed, they require a hard mask, and significantly increase the fabrication steps needed for etching the material as well as slightly increasing the surface roughness [14], [15]. Hence, neither of the above-mentioned methods are promising solutions for frequency scaling thin-film $LiNbO_3$. Meanwhile, an inductively coupled plasma etching mechanism, in which the ions are accelerated remotely, possesses potential for such applications. Here, we propose a method to avoid fabrication difficulties by transferring piezoelectric material onto a substrate at a reasonable thickness, ensuring the quality and the uniformity of the film, followed by ion beam assisted Argon gas cluster etching for scaling the film to thicknesses necessary for high–frequency operation whilst maintaining performance specifications.

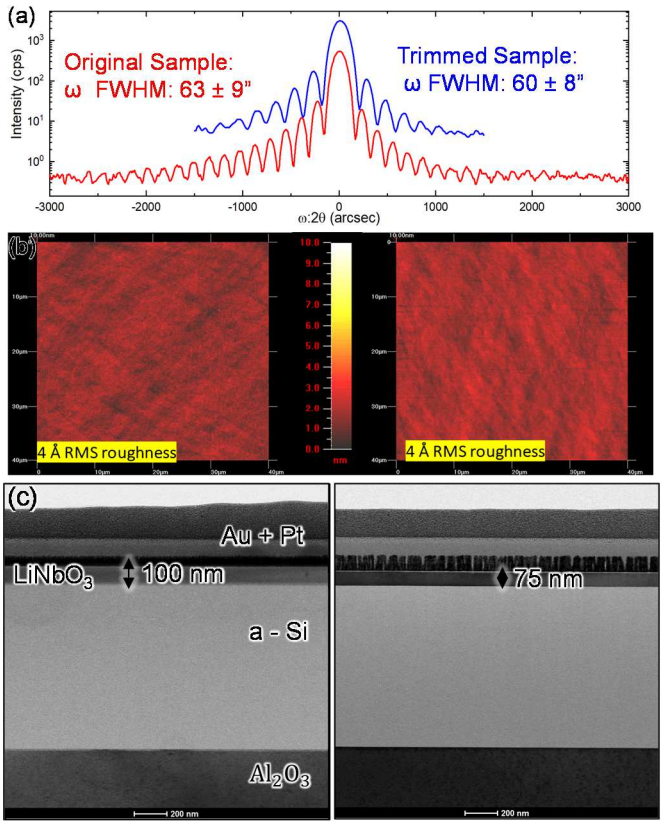

Fig. 1. (a) TAXRD (ω values from ω-scans), (b) AFM of the original and trimmed $LiNbO_3$ thin films, (c) TEM image of the original stack,, and the TEM image of the trimmed stack.

II. Methods/Results

A 100 nm thick $LiNbO_3$ on 1 µm amorphous silicon (Si) on Sapphire substrate was provided by NGK Insulators Ltd. The

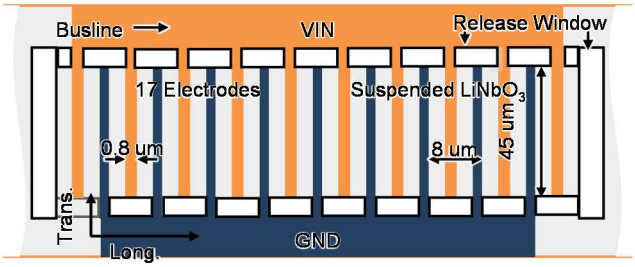

Fig. 2. Top view of fabricated resonator design with key parameters labeled.

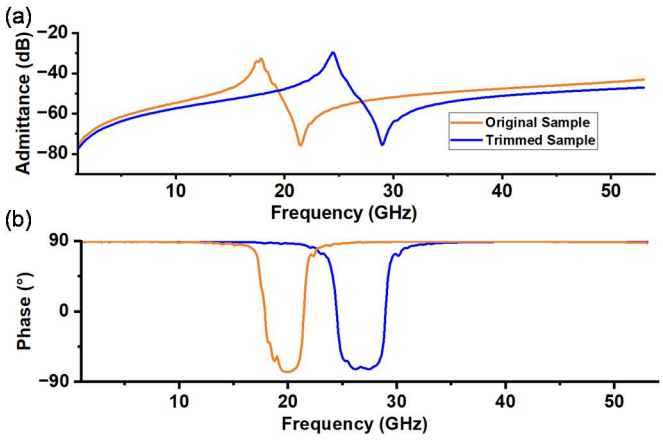

Fig. 3 FEA simulated admittance (a) amplitude and (b) phase for the 100 nm and 75 nm $LiNbO_3$ thin film stack.

film was trimmed at normal incidence from 100 nm to 75 nm using the AJA Ion Mill with 6 SCCM of Argon gas flow, and a 300 Volt ion beam bias with an etch rate of 1.3 nm/min. The sample was mounted using copper tape on a rotating substrate carrier with substrate cooling for the purpose of axis-symmetry and minimization of thermal damage induced in the film. The material-level crystal analysis, namely Triple Axis X-Ray Diffraction (TAXRD), Atomic Force Microscopy (AFM), and Transmission Electron Microscopy were performed prior to and after the trimming, showing an equally well-aligned crystal and a smooth film surface [Fig. 1 (a)(b)]. Hence, the ion beam trimming process effectively thins the film whilst imparting minimal damage.

Next, acoustic resonators with interdigitated electrodes (IDT) were designed on both the original and trimmed $LiNbO_3$ [16]. Sample device design can be seen in Fig. 2. A sample device was simulated using finite element analysis (FEA) to study device performance at both the original and trimmed thicknesses [Fig. 3 (a)(b)]. Simulations indicated that the first-order antisymmetric (A1) resonance at the original film thickness occured at 17 GHz, while the same mode occured at 24 GHz in the trimmed film - the traversal of this frequency range scaled the device into mm-wave frequency band. As a result, the resonators are then fabricated [Fig. 4 (a)], and their optical images can be seen in Fig. 4. (b)(c).

Fabricated resonators yielded varying characteristics as their electrode widths differed (0.4 – 1.6 µm) while their inter-electrode width (8 µm) and transducer cell number were maintained. As a result, piezoelectric material surface

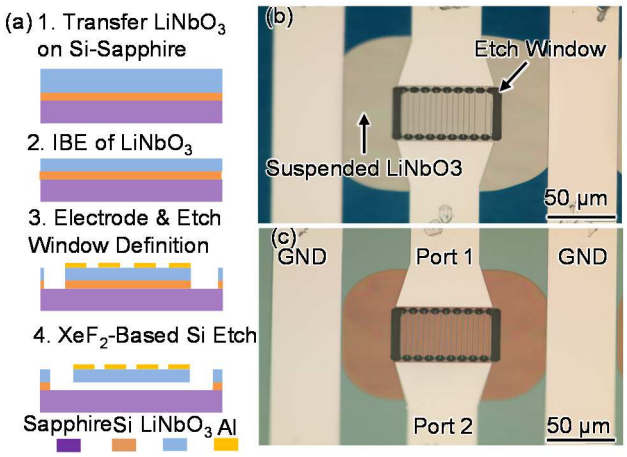

Fig. 4 (a) Fabrication flowchart. Optical image of a resonator fabriated with (b) the trimmed thickness film, and (c) original thickness film.

metallization was the major factor changing between each fabricated device.

Following fabrication, the devices were measured with a vector network analyzer (VNA). Measurements at the original thickness indicated resonances in the range of 16.8 – 17.5 GHz. The trimmed samples were found to exhibit resonant peaks ranging from 24.4 to 25.1 GHz with an FoM ranging from 9 – 18.5. The measurements of a device group with an identical design (0.8 µm electrode width) at varying film thicknesses is plotted in Fig. 5, with Butterworth Van-Dyke equivalent circuit parameters extracted.

III. DISCUSSION

The overall comparison of all devices in the original and trimmed films are plotted in Fig. 6, showing key specifications including f, Q, $f{\cdot}Q$, and $f{\cdot}Q{\cdot}k^2$. The scatter plot of the resonant frequencies shows that trimming achieved frequency scaling [Fig. 6 (a)]. The quality factor along with $f{\cdot}Q$, and $f{\cdot}Q{\cdot}k^2$ are also plotted as they represent key parameters often used to assess the performance of an acoustic resonator [Fig. 6 (b)(c)], as well as the quality of the material used to fabricate one. Hence, the maintenance of a similar $f{\cdot}Q$ product indicates that the piezoelectric film quality has been maintained, which is in agreement with earlier material level testing [Fig. 1]. Moreover, the trimming process did not affect k^2 and thus a high $f{\cdot}Q{\cdot}k^2$ is maintained [Fig. 6 (d)]. The reduction in the quality factor of the acoustic resonators at ultra-thin dimensions or due to wider electrodes is to be expected. As the film thickness was reduced, so was the volume available for storing energy within the device, reducing its quality factor. Similarly, for the proposed IDT geometry, wider electrodes reduced the active area of the device and reduced the amount of charge being generated due to piezoelectricity. On the other hand, poor performance was noted for devices with narrow electrodes on the original film, which improved in the trimmed film. As the device's active area was larger for those with less metalization, this statistic could be attributed to potential defects in the piezoelectric film which were then removed during the trimming process.

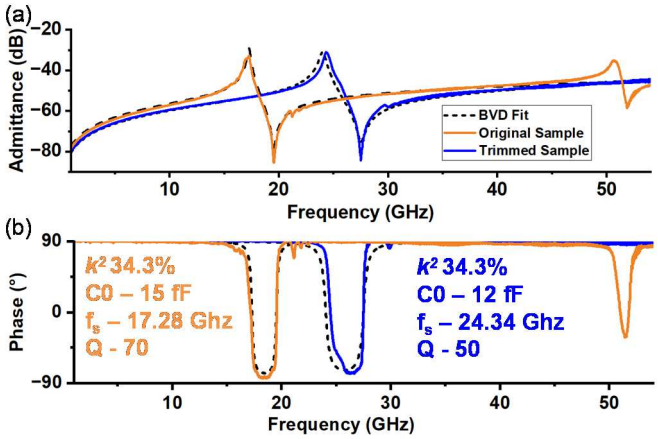

Fig.5 BVD fit and VNA measurements of (a) admittance and (b) phase for both 100 nm and 75 nm samples, along with extracted BVD parameters.

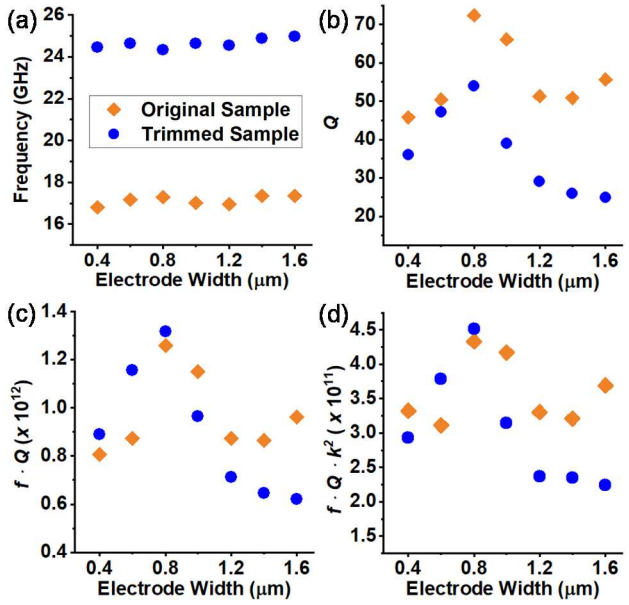

Fig. 6 Scatter charts of (a) frequency (*f*), (b) *Q*, (c) *f*·*Q*, (d) *f*·*Q*·k^2 against the group of devices with different electrode widths.

Not only did the proposed fabrication step yield satisfactory results, it also possesses significant potential for improvement given the degree of freedom for further optimization of the trimming recipe. The trimming performed here occurs at normal incidence using argon gas ionised at constant low power. Meanwhile, the carrier substrate tilt, the ion beam bias voltage, and current can all be tailored to customize the etch rate, etch profile, the electrostatic, and thermal effects induced in the ion beam etching chamber. Each of these options must be carefully considered as they possess unique effects that could either enhance, or adversely affect the fabrication step.

The incidence angle of the collimated ion beam onto the substrate is a major factor in determining the etch rate for the chosen material. The etching rate increases for most materials from normal incidence to the range of 40°- 60°. This is likely due to the increase in the likelihood of an atom obtaining momentum directed away from the sample surface as a result of the momentum transfer between itself and an ion from the

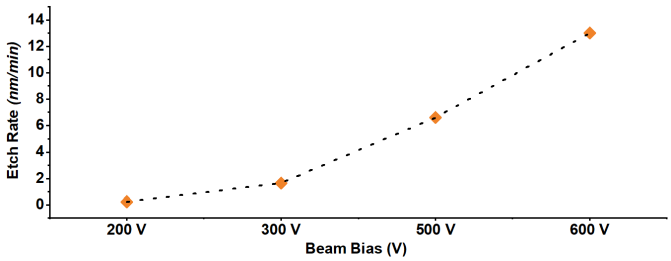

Fig. 7 Etch rate for $LiNbO_3$ at normal incidence as a function of ion beam voltage while keeping ion current density below the ion impingement limit for the AJA Ion Mill.

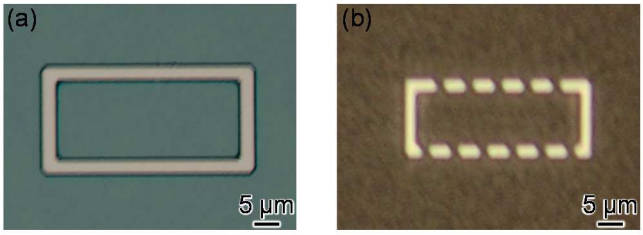

Fig. 8 (a) An optical image of an etch window on $LiNbO_3$ trimmed at 300 Volt ion beam bias, (b) an optical image of a similar but different etch window on $LiNbO_3$trimmed at 600 Volt ion beam bias.

collimated beam. The etch rate falls off again past this angle since the beam is now exposed to a larger effective area of the sample surface [16], [17].

The ion beam bias voltage and the ion beam current play a significant role in determining the quality of the material following the processing step. The etch rate increases somewhat linearly in the bias voltage range of 300 – 1000 V [Fig. 7], however, it drops off drastically once the beam is biased below 300 V [12], [18]. Electrostatic damage to the substrate, even at high power, is avoided since the ion beam space charge is largely canceled due to electrons from the neutralizer in the chamber, allowing the etch profile to be maximally smooth [19], [20]. Meanwhile, thermal damage due to ion bombardment is usually mitigated by using substrate cooling. In this work, since the trimming occurs on the top surface of a substrate stack with poor thermal conductivity, the substrate cooling mechanism may be unable to prevent thermal damage effectively. Hence, the bonding method between the sample and the sample carrier must be optimized. In other cases, thermal issues could lead to burning of soft photoresist [Fig. 8]. This drawback could be avoided with the use of a hard mask, though this would then increase the complexity of the fabrication process [21], [22]. Nonetheless, this issue does not concern frequency scaling thin films as a layer of photoresist is not necessary whilst trimming the film.

Yet another important effect induced by the ion beam etching method is the material re-deposition effect. While this effect could be detrimental, it proved to be helpful for this work. As atoms are ejected from the sample surface due to momentum transfer, a portion of them are deposited on the sidewalls of the photoresist being used to define the etch window. As a result, ridges are formed at the border of each etch window following the process [Fig. 9]. The formation of said ridges can be minimized by rounding the edges of the photoresist layer by over-baking it, or by cleaning the sample surface using a chemical solution post-etch [16], [23], [24]. However, without

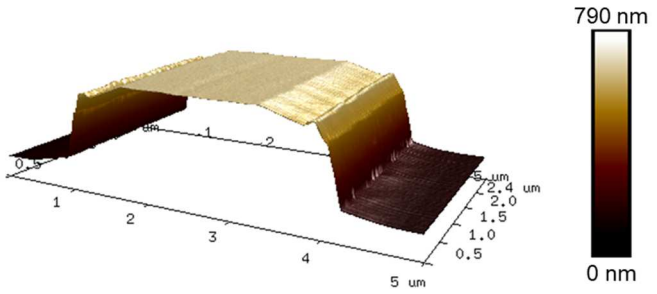

Fig. 9 An etch window profile after ion beam assisted argon gas cluster etching acquired using Atomic Force Microscopy, demonstrating the material re-deposition effect.

photoresist, the re-deposited material will tend to fill troughs on the material surface, improving, or maintaining the surface roughness of the sample in question [25], [26]. For $LiNbO_3$ this indicates that the film quality will be maintained, whereas for materials with inherently poor surface roughness, such as AlN and ScAlN, the film quality could be improved through the ion beam trimming process [Fig 1. (b)], [27], [28].

On another note, if local frequency tuning needs to be performed, the slow etching, low power (<300 V) operation of the ion beam would be successful. This configuration allows notoriously fragile mechanical structures, such as suspended acoustic resonators, to maintain their performance characteristics while scaling them in frequency [29].

IV. Conclusions

As demonstrated, ion beam assisted argon gas cluster trimming of thin films to ultra-thin dimensions allows for frequency scaling of acoustic resonators whilst maintaining key performance parameters of the device and the film quality. This method with minimal parametrization is readily a viable path towards obtaining a 24.3 GHz resonator with an FoM of 18.5, a result rivaling high-performance designs at a similar operating frequency. Hence, further optimizing the trimming recipe to trimming $LiNbO_3$ or other piezoelectric thin films - especially those with inherently poor surface roughness and thermal characteristics - will likely improve the results seen here.

References

[1] S. Gong, R. Lu, Y. Yang, L. Gao, and A. E. Hassanien, "Microwave Acoustic Devices: Recent Advances and Outlook," *IEEE Journal of Microwaves*, vol. 1, no. 2, pp. 601–609, Apr. 2021,

[2] K. P. Jackson *et al.*, "Optical Fiber Delay-Line Signal Processing."

[3] R. Lu and S. Gong, "RF acoustic microsystems based on suspended lithium niobate thin films: Advances and outlook," *Journal of Micromechanics and Microengineering*, vol. 31, no. 11. IOP Publishing Ltd, Nov. 01, 2021.

[4] Y. Yang, R. Lu, L. Gao, and S. Gong, "10-60-GHz Electromechanical Resonators Using Thin-Film Lithium Niobate," *IEEE Trans Microw Theory Tech*, vol. 68, no. 12, pp. 5211–5220, Dec. 2020,

[5] X. Bai *et al.*, "The thin film bulk acoustic wave resonator based on single-crystalline 4 3 - Ɔ Y-cut lithium niobate thin films," *AIP Adv*, vol. 10, no. 7, Jul. 2020,

[6] R. Wang, S. A. Bhave, and K. Bhattacharjee, "Design and fabrication of S0 Lamb-wave thin-film lithium niobate micromechanical resonators," *Journal of Microelectromechanical Systems*, vol. 24, no. 2, pp. 300–308, Apr. 2015,

[7] G. Piazza, P. J. Stephanou, and A. P. Pisano, "Piezoelectric aluminum nitride vibrating contour-mode MEMS resonators," *Journal of Microelectromechanical Systems*, vol. 15, no. 6, pp. 1406–1418, Dec. 2006,

[8] R. Ruby, "FBAR-From Technology Development to Production."

[9] M. Akiyama, T. Kamohara, K. Kano, A. Teshigahara, Y. Takeuchi, and N. Kawahara, "Enhancement of piezoelectric response in scandium aluminum nitride alloy thin films prepared by dual reactive cosputtering," *Advanced Materials*, vol. 21, no. 5, pp. 593–596, Feb. 2009,

[10] S. Yoshida *et al.*, "REACTIVE MOLECULAR BEAM EPITAXY OF ALUMINIUM NITRIDE.," *Journal of vacuum science & technology*, vol. 16, no. 4, pp. 990–993, 1979,

[11] J. Kramer *et al.*, "57 GHz Acoustic Resonator with k2of 7.3 % and Q of 56 in Thin-Film Lithium Niobate," in *Technical Digest - International Electron Devices Meeting, IEDM*, Institute of Electrical and Electronics Engineers Inc., 2022, pp. 1641–1644.

[12] S. Y. Siew *et al.*, "Ultra-low loss ridge waveguides on lithium niobate via argon ion milling and gas clustered ion beam smoothening," *Opt Express*, vol. 26, no. 4, p. 4421, Feb. 2018,

[13] C. M. Chang *et al.*, "A parametric study of ICP-RIE etching on a lithium niobate substrate," in *2015 IEEE 10th International Conference on Nano/Micro Engineered and Molecular Systems, NEMS 2015*, Institute of Electrical and Electronics Engineers Inc., Jul. 2015, pp. 485–486.

[14] H. Hui, R. Ricken, and W. Sohler, "Etching of Lithium Niobate: From Ridge Waveguides to Photonic Crystal Structures."

[15] R. Zhuang, J. He, Y. Qi, and Y. Li, "High-Q Thin-Film Lithium Niobate Microrings Fabricated with Wet Etching," *Advanced Materials*, vol. 35, no. 3, Jan. 2023,

[16] R. E. Lee, "MICROFABRICATION BY ION-BEAM ETCHING.," *J Vac Sci Technol*, vol. 16, no. 2, pp. 164–170, 1979,

[17] D. W. YOUNGNER and C. M. HAYNES, "MODELING ION BEAM MILLING.," *J VAC SCI TECHNOL*, vol. V 21, no. N 2, pp. 677–680, 1982,

[18] D. M. Demidov, R. V Leus, and V. P. Chaly, "Dry etching of aluminum nitride by an ion beam," 1997.

[19] R. James, Y. Pilloux, and H. Hegde, "Reactive ion beam etching of piezoelectric ScAlN for bulk acoustic wave device applications," in *Journal of Physics: Conference Series*, Institute of Physics Publishing, Dec. 2019.

[20] R. M. R. Pinto, V. Gund, C. Calaza, K. K. Nagaraja, and K. B. Vinayakumar, "Piezoelectric aluminum nitride thin-films: A review of wet and dry etching techniques," *Microelectronic Engineering*, vol. 257. Elsevier B.V., Mar. 15, 2022.

[21] C. Chia, B. Machielse, A. Shams-Ansari, and M. Lončar, "Development of hard masks for reactive ion beam angled etching of diamond," *Opt Express*, vol. 30, no. 9, p. 14189, Apr. 2022,

[22] S.-W. Chun, D. Kim, J. Kwon, B. Kim, H. Lee, and S.-B. Lee, "Negative electron-beam resist hard mask ion beam etching process for the fabrication of nanoscale magnetic tunnel junctions," *Journal of Vacuum Science & Technology B, Nanotechnology and Microelectronics: Materials, Processing, Measurement, and Phenomena*, vol. 30, no. 6, p. 06FA01, Nov. 2012,

[23] J. K. Hirvonen and J. K. Hirvonen, "Ion beam assisted thin film deposition," 1991.

[24] K. P. Miiller and J. Pelka, "Redeposition in ion milling," 1987.

[25] T. Shima and N. Inoue, "A study on surface roughness in ion-beam machining," 1990.

[26] F. Frost, R. Fechner, B. Ziberi, J. Völlner, D. Flamm, and A. Schindler, "Large area smoothing of surfaces by ion bombardment: Fundamentals and applications," *Journal of Physics Condensed Matter*, vol. 21, no. 22, 2009,

[27] J. Tang, D. Niu, Z. Tai, and X. Hu, "Deposition of highly c-axis-oriented ScAlN thin films at different sputtering power," *Journal of Materials Science: Materials in Electronics*, vol. 28, no. 7, pp. 5512–5517, Apr. 2017,

[28] S. Cho et. al., "*28.4 Ghz Thin Film Bulk Acoustic Resonator in Thin-Film Scandium Aluminum Nitride,*" International Ultrasound Symposium, 2023

[29] V. Chulukhadze et. al., "*Frequency Tuning of Suspended Millimeter Wave Lithium Niobate Acoustic Resonators by Ion Beam Assisted Argon Gas Cluster Trimming,*" International Ultrasound Symposium, 2023